

Supplemental information: Self-assembly of dodecagonal and octagonal quasicrystals in hard spheres on a plane

E. Fayen, M. Impérator-Clerc, L. Filion, G. Foffi, F. Smallenburg

FINAL CONFIGURATIONS

An archive of simulated final configurations for the data set depicted in Figure 3 of the main text is provided at <https://doi.org/10.5281/zenodo.7712001> via Zenodo. In particular, we provide a zipped archive of the final configurations, snapshot images, and diffraction patterns for all simulations performed using $N = 2000$ particles. The files are organized into folders and accompanied by HTML documents which allow for a rapid visualization of all simulation results for a single size ratio.

HEX_L⁺ PHASE AT DIFFERENT COMPOSITIONS

As mentioned in the main text, we use the label Hex_L⁺ to refer to any phase consisting of a hexagonal lattice of large spheres interspersed with small spheres, regardless of the ordering of the smaller spheres. In Fig. 1, we show snapshots for a range of different compositions. The hexagonal symmetry of the large-sphere lattice remains in place even though the concentration of small spheres varies drastically. For low compositions x_S , only a few small spheres are randomly interspersed in the triangular holes in the lattice. This concentration increases all the way up to $x_S \simeq 2/3$, at which point all triangular holes in the lattice are filled, corresponding to the T1 crystal phase. Above this concentration, the large particles start to become more separated, as additional small particles fill the gaps between them. While this leads to local lattice distortions and a decrease in hexagonal ordering (e.g. at $x_S = 0.7$), overall the system maintains its hexagonal symmetry. In principle, pushing these systems to larger packing fractions may stabilize more ordered phases, such as those predicted by the infinite-pressure phase diagram in the main text. However, these high-density phases are likely hard to reach via spontaneous self-assembly due to the kinetic arrest that occurs at high packing fractions.

TILING ANALYSIS

The quasicrystalline phases can be rationalised as tilings of the plane by decorated tiles. To identify the underlying tiling in simulation snapshots, we first create bonds between all large particles within a cutoff distance of $1.3\sigma_{LL}$ for QC12 and $1.7\sigma_{LL}$ for QC8 systems. Since the QC8 contains short and long bonds, the long cutoff distance required to capture long bonds also generates crossing bonds within S1 tiles, which need to be removed. Tiles are then reconstructed from cycles in the bond network, and sorted by shape and orientation.

To characterise the neighbour network, we compute the bonds length and angle distributions, as shown in Figure 2. Bond angles are relative to the horizontal. In the vicinity of the QC8 region, the bond length distribution is clearly bimodal. A cutoff is set at the minimum of the distribution in-between the two peaks, which discriminates between long and short bonds. Since the cutoff value can vary slightly with the composition and packing fraction of the system, we determine it automatically for each snapshot. The bond angle distribution exhibits 16 sharp peaks centered on the directions of an ideal tiling of large squares, small squares and equilateral triangles. Correlating the orientation with the bond length shows that short and long bonds each follow a distinct set of 8 orientations, offset by $\pi/8$.

TILES FRACTIONS IN QC8

For the square-triangle tiling associated with the QC12 phase, it is well known that global twelve-fold symmetry only occurs under the condition that the two area fractions of the tiling covered by squares and triangles are the same and equal to $1/2$ [1, 2]. Here, we determine under what conditions the QC8 phase can exhibit 8-fold symmetry. To this end, we consider a QC8 tiling consisting of large squares S , small squares s , and triangles T , with long edge length a . Counting the different orientations, this results in a total of 12 different tiles: two orientations of both types of squares, and 8 orientations of the triangles. These are listed in Table I. We then consider an infinite, globally

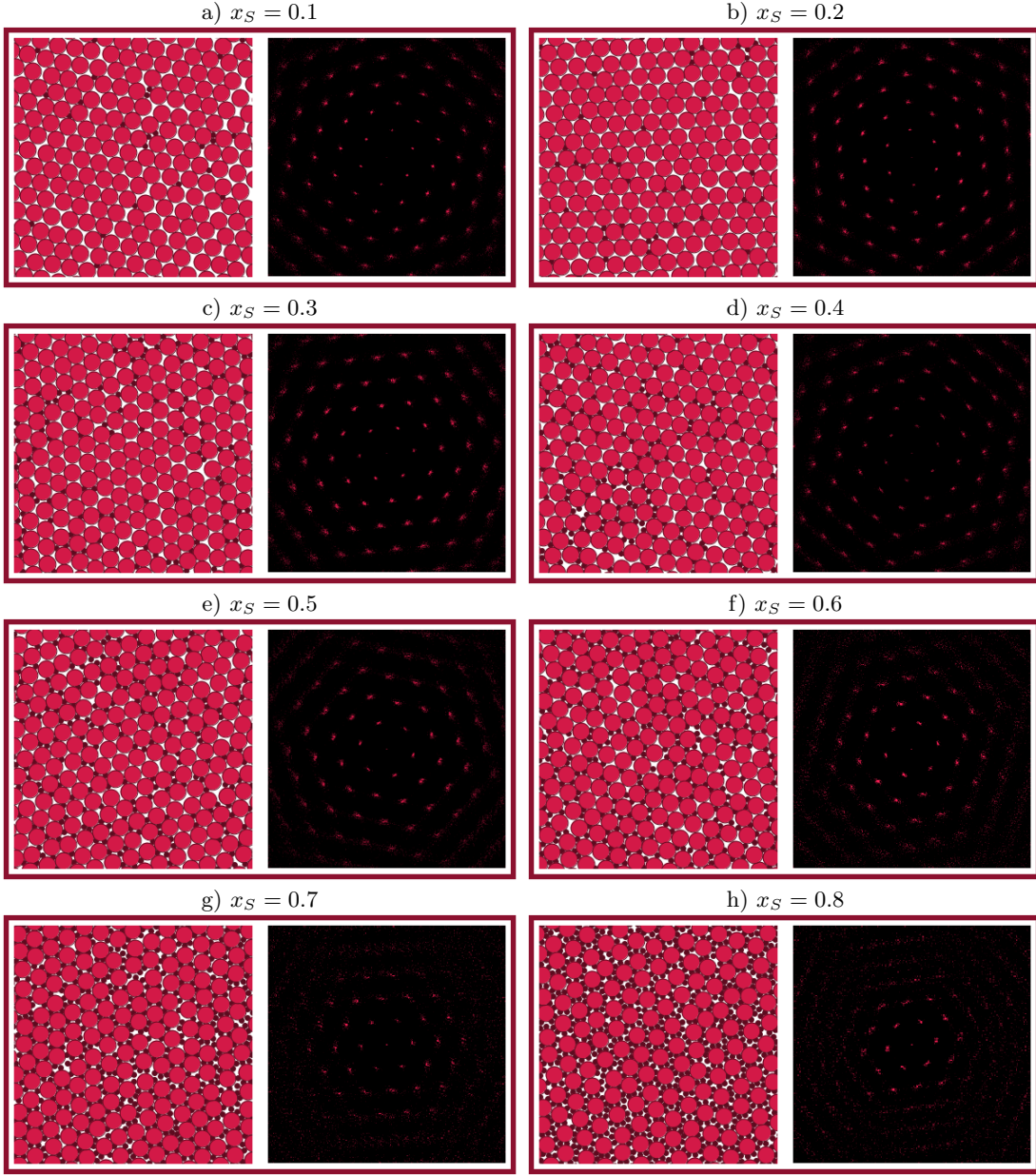


FIG. 1. Variations of the Hex_L^+ phase, at size ratio $q = 0.35$ and varying compositions x_S . The packing fractions for the snapshots vary from $\eta = 0.82$ in (a) to $\eta = 0.96$ in (h), in steps of 0.02.

uniform[2] tiling consisting of a mixture of these tiles, with the area fraction covered by each tile type denoted as Σ_i for the large squares, σ_i for the small squares, and τ_i for the triangles, where i denotes the orientation of the tile.

The first obvious constraint on our tiling is that it should cover the entire plane. Hence, the area fractions must satisfy

$$\Sigma + \sigma + \tau = 1, \quad (1)$$

where $\Sigma = \sum_i \Sigma_i$, $\sigma = \sum_i \sigma_i$, and $\tau = \sum_i \tau_i$.

One set of constraints on these tile concentrations follows from the simple observation that each edge must have an opposing partner. Considering, for example, the short edge in triangle T_1 , this leads to the constraint that

$$n_{T_1} + n_{s_1} = n_{T_5} + n_{s_1}, \quad (2)$$

with n_{X_i} denotes the number of tiles of type X_i . This trivially implies that $\tau_1 = \tau_5 = \tau_{15}/2$, and likewise it can be shown that $\tau_2 = \tau_6 = \tau_{26}/2$, $\tau_3 = \tau_7 = \tau_{37}/2$, and $\tau_4 = \tau_8 = \tau_{48}/2$.

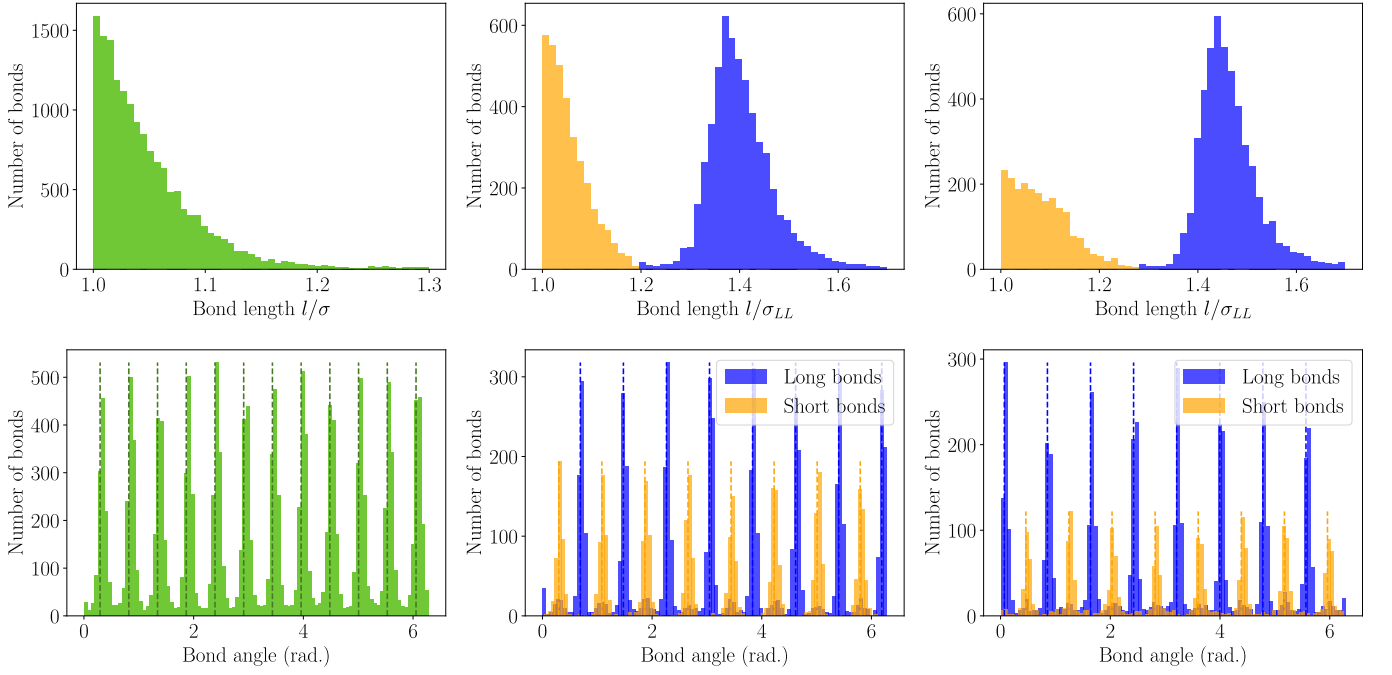


FIG. 2. Neighbour bonds characterisation in systems of 10^4 non-additive hard disks, with size ratio $q = 0.45$, composition $x_S = 0.35$ and packing fraction $\eta = 0.84$ (Left), $q = 0.5$, $x_S = 0.675$, $\eta = 0.86$ (Centre) and $q = 0.55$, $x_S = 0.725$, $\eta = 0.84$ (Right). The first system forms a dodecagonal random tiling quasicrystal, while the two last ones form octagonal random tiling quasicrystals. (Top) Bonds length distributions show a clear distinction between short and long bonds in octagonal tilings. (Bottom) Bond angle distributions.

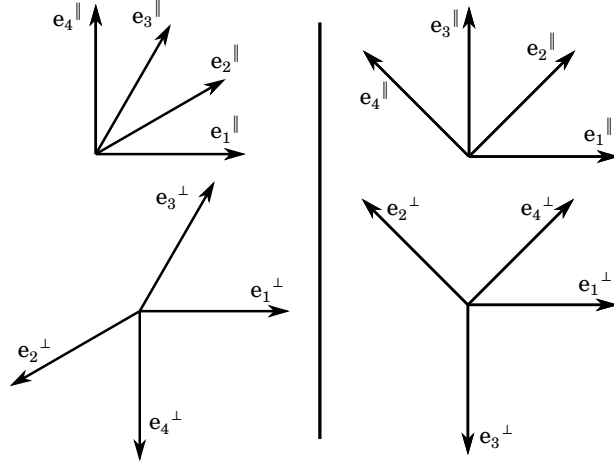


FIG. 3. Projections of the 4D lift vectors on the parallel and perpendicular sub-spaces for the square-triangle (Left) and large square-small square-isosceles triangle (Right) tilings.

Another constraint on the various tile concentrations can be obtained by using the four-dimensional representation of the tilings. For this, we follow the procedure outlined in e.g. [1–3]. In particular, in the QC8 tiling, each long edge can only lie along one of 4 different orientations \mathbf{e}_1 through \mathbf{e}_4 , illustrated in Fig. 3(left). Short edges can then be constructed by taking the difference between two of these vectors (e.g. $\mathbf{e}_2 - \mathbf{e}_1$). As a result, each vertex in our tiling can be written as a linear combination of an integer number of the four vectors \mathbf{e}_i , and hence can be seen as a point on a four-dimensional lattice. We then associate each vector \mathbf{e}_i with a corresponding vector \mathbf{e}_i^\perp , illustrated in Fig. 3(right), such that each vertex in the tiling can be uniquely associated with a point in the perpendicular space [3, 4].

We can then consider a mapping $\phi(\mathbf{r})$ that maps each vertex in our original tiling to its corresponding point in the perpendicular space. Within each tile, $\phi(\mathbf{r})$ is a linear interpolation between the mapped vertices of that tile. Hence, ϕ is a continuous, piecewise linear function, with a constant hyperslope within each tile. The hyperslope within one


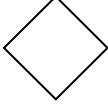
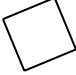
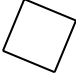
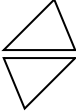
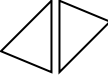


Name	Tile	Area A_{X_i}	Hyperslope B_{X_i}	$\det B_{X_i}$
S_1		a^2	$\begin{pmatrix} 1 & 0 \\ 0 & -1 \end{pmatrix}$	-1
S_2		a^2	$\begin{pmatrix} -1 & 0 \\ 0 & 1 \end{pmatrix}$	-1
s_1		$(2 - \sqrt{2})a^2$	$(1 + \sqrt{2}) \begin{pmatrix} 0 & -1 \\ -1 & 0 \end{pmatrix}$	$-3 - 2\sqrt{2}$
s_2		$(2 - \sqrt{2})a^2$	$(1 + \sqrt{2}) \begin{pmatrix} 0 & 1 \\ 1 & 0 \end{pmatrix}$	$-3 - 2\sqrt{2}$
$T_{1,5}$		$\frac{1}{2\sqrt{2}}a^2$	$\begin{pmatrix} 1 & -2 \\ 0 & 1 \end{pmatrix}$	1
$T_{2,6}$		$\frac{1}{2\sqrt{2}}a^2$	$\begin{pmatrix} -1 & 0 \\ 2 & -1 \end{pmatrix}$	1
$T_{3,7}$		$\frac{1}{2\sqrt{2}}a^2$	$\begin{pmatrix} -1 & 0 \\ -2 & -1 \end{pmatrix}$	1
$T_{4,8}$		$\frac{1}{2\sqrt{2}}a^2$	$\begin{pmatrix} 1 & 2 \\ 0 & 1 \end{pmatrix}$	1

TABLE I. Summary of the 12 different tiles comprising the QC8 tiling. The third column reports the area of each tile, assuming that large squares have edges of length a . The fourth column contains the constant hyperslope of each tile, *i.e.* the 2x2 matrix that maps points inside that tile in the original tiling to the perpendicular space. The last column displays the determinant of the hyperslope for each tile, which is used to obtain Eq 6.

tile is completely determined by the vectors that form it. Hence, tiles of the same type and orientation have the same hyperslope. Specifically, within a tile X_i , the hyperslope B_{X_i} is given by:

$$B_{X_i} = \begin{pmatrix} \frac{\partial \phi_x}{\partial x} & \frac{\partial \phi_x}{\partial y} \\ \frac{\partial \phi_y}{\partial x} & \frac{\partial \phi_y}{\partial y} \end{pmatrix}. \quad (3)$$

In Table I, we report the hyperslope for each of the 12 tiles in the QC8 tiling.

In a globally uniform tiling, over long distances \mathbf{r} , $\phi(\mathbf{r})$ has a well-defined average hyperslope B (also known as the global perpendicular strain), which can be written as the weighted sum of the hyperslopes of the individual tiles [2]:

$$B = \sum_{i=1}^2 \Sigma_i B_{S_i} + \sum_{i=1}^2 \sigma_i B_{s_i} + \sum_{i=1}^8 \tau_i B_{T_i}. \quad (4)$$

Following Ref. [2], uniformity of the tiling then imposes that

$$\sum_{i=1}^2 \Sigma_i \det B_{S_i} + \sum_{i=1}^2 \sigma_i \det B_{s_i} + \sum_{i=1}^8 \tau_i \det B_{T_i} = \det B. \quad (5)$$

Using the matrices listed in Table I, this leads to the following constraint:

$$\Sigma + (3 + 2\sqrt{2})\sigma - \tau = (\Sigma_1 - \Sigma_2)^2 + (3 + 2\sqrt{2})(\sigma_1 - \sigma_2)^2 - \tau^2 + (2 + 2\sqrt{2})(\tau_{15} - \tau_{26} + \tau_{37} - \tau_{48})(\sigma_1 - \sigma_2) + 8(\tau_{15}\tau_{37} + \tau_{26}\tau_{48}). \quad (6)$$

This constraint can be regarded as the equivalent of the Nienhuis relation [2, 5] for the (QC12) square-triangle tiling, but for our QC8 tiling.

For a maximally symmetric tiling with eight-fold symmetry, the requirement is that all orientations of each tile appear in the same amount [2]. In other words:

$$\Sigma_1 = \Sigma_2 = \frac{\Sigma}{2} \quad (7)$$

$$\sigma_1 = \sigma_2 = \frac{\sigma}{2} \quad (8)$$

$$\tau_{15} = \tau_{26} = \tau_{37} = \tau_{48} = \frac{\tau}{4}. \quad (9)$$

When we impose this, the average hyperslope B vanishes (zero perpendicular strain), and as a result the right-hand side of Eq. 6 similarly becomes zero, yielding:

$$\Sigma + (3 + 2\sqrt{2})\sigma - \tau = 0. \quad (10)$$

Finally, we can express the area fractions Σ , σ and τ in terms of the particle composition x_S by using the known composition of each tile, combined with equations 1 and 10 (see equations 3, 4 and 5 of the main text).

LIFT TO 4D AND PERPENDICULAR STRAIN

Mapping a tiling to its higher dimensional representation is called *lifting*. This procedure gives access to valuable information for the analysis of quasicrystals. In particular, the relationship between the distances in perpendicular and parallel projections can be used to measure the perpendicular strain of the structure at hand.

In practice, lifting a structure amounts to assigning each vertex to a points in a higher dimensional space. The lift spaces of both square-triangle and large square-small square-isosceles triangle tilings are 4-dimensional, but with different basis vectors. In Figure 3, we report the parallel and perpendicular projections of the lift vectors used to analyse our tilings. We use the standard lift basis for the square-triangle tiling [2]. The vectors used to lift the large square-small square-isosceles triangle tilings are the those commonly used for lifting the Ammann-Beenker or Watanabe-Ito-Soma tilings [6, 7].

After reconstruction of the tilings, we lift the tiling recursively from a starting point, tile after tile. We find that lifting the tiling tile after tile rather than bond after bond is more robust. Indeed, we lift only tiles that unambiguously correspond to one of the allowed orientation, thus preventing the ambiguous orientation of a single bond to propagate further in the recursive lifting. During the lift construction, we ignore the periodic boundary conditions of the simulation box.

Once a tiling is lifted, projecting back onto the parallel subspace yields a “rectified” tiling with no thermal noise, where all tiles have their ideal shape as illustrated in Figure 4-top. The rectified tilings contain small defects that are local and do not disrupt the tiling further away, as well as long defect lines that nucleate at topological defects and separate islands of tiling. Interestingly these “tears” defects were previously observed by Joseph and Elser in a simple growth model for the QC12 tiling of squares and triangles [8]. One can also project the lifted vertices to the perpendicular subspace 4-bottom. The perpendicular projection gives indication about the quality of the quasicrystal. In an ideal dodecagonal quasicrystal, the vertices form a fractal-shaped pattern with 12-fold symmetry. In a random tiling quasicrystal, this shape is blurred somewhat, but remains compact. Here, because of the many defects in the tiling, we observe that the points spread away from the origin. Nonetheless, we note that the perpendicular projections form a very dense cluster (note the different scales for perpendicular and parallel axis), a signature of quasicrystalline structures.

With both parallel and perpendicular coordinates of each vertex, we can compute the perpendicular strain of the self-assembled tilings. By binning the pair particle distances in parallel space, we compute the perpendicular displacement field as explained in the main text [9], and measure the average perpendicular strain ξ as the slope of the linear regime, as illustrated in the main text. We compare these average perpendicular strains with those of reference periodic structures. For the square-triangle tilings, we take the first approximant to the dodecagonal quasicrystal (the sigma phase, see Figure 5-Left) as a reference structure of average perpendicular strain $\xi_{\text{ref}} = 2\sqrt{2} - \sqrt{6} \approx 0.38$. For the large square-small square-isosceles triangle tilings, we use a square lattice decorated with octagons as our reference periodic structure. The octagon can host various clusters as depicted in Figure 5-Right thus allowing to construct periodic structures with different tiles concentrations. This family of periodic structure all have an average perpendicular strain of $\xi_{\text{ref}} = 3\sqrt{2} - 4 \approx 0.24$.

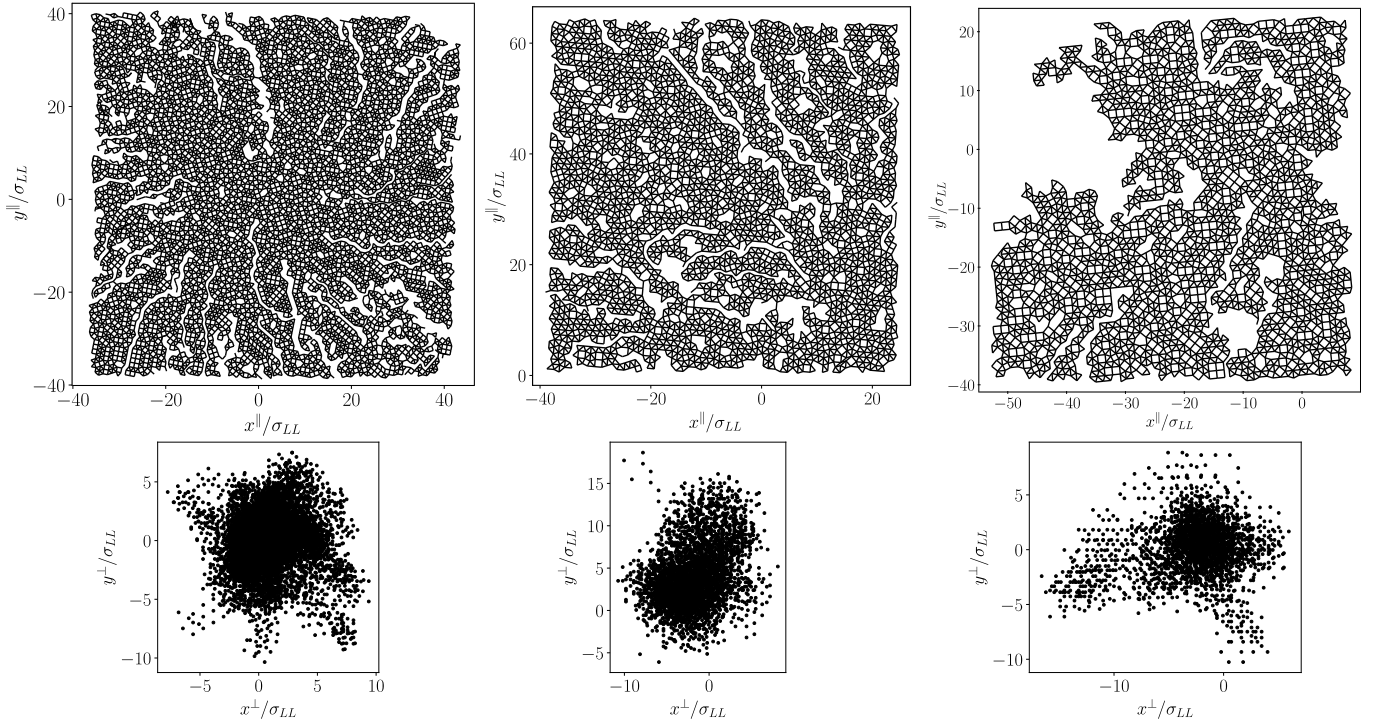


FIG. 4. Parallel (Top) and perpendicular (Bottom) projections of the lifted tilings. (Left) QC12 $q = 0.45$, $x_S = 0.35$, $\eta = 0.84$. (Centre) QC8 $q = 0.5$, $x_S = 0.675$, $\eta = 0.86$. (Right) QC8 $q = 0.55$, $x_S = 0.725$, $\eta = 0.84$. The empty region in to top right corner corresponds to a fluid pocket with no tiling structure.

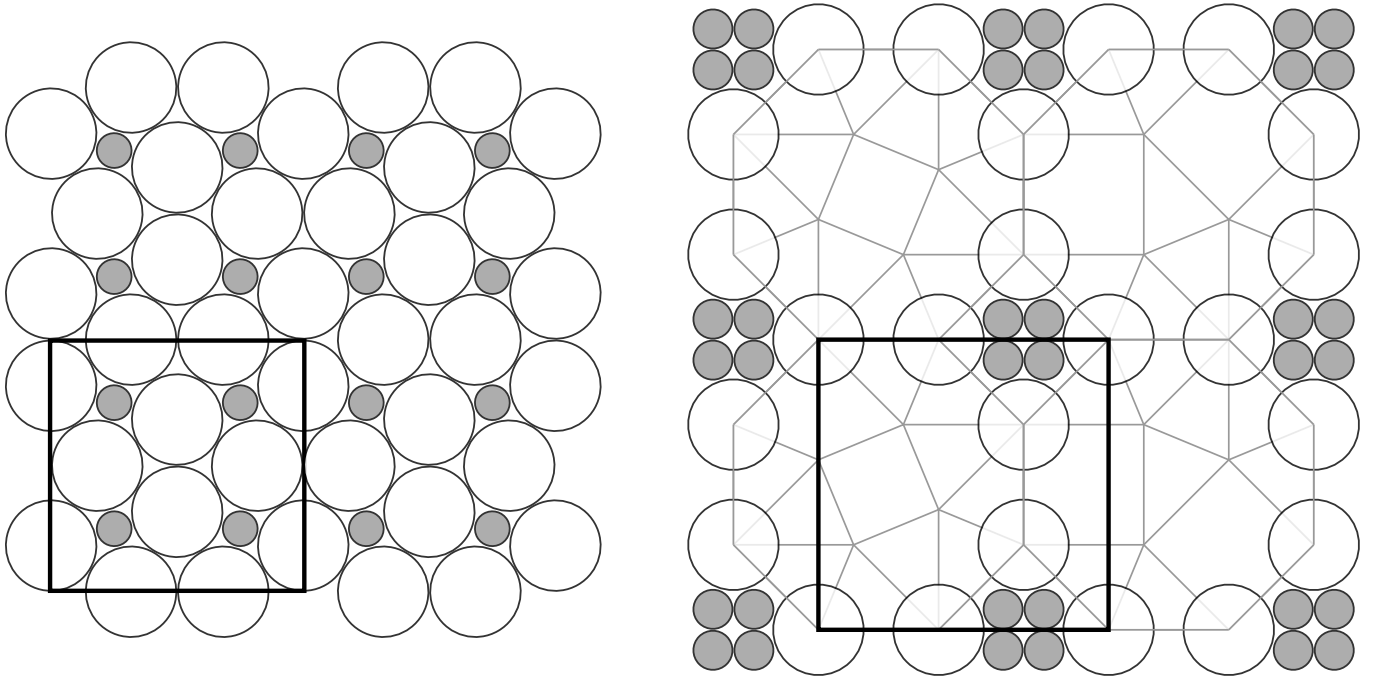


FIG. 5. Reference periodic phases. Black squares highlight the unit cells. (Left) The sigma phase, first approximant of the dodecagonal tiling. (Right) A reference periodic structure based on the large square-small square-isosceles triangle tiling. The octagons can host cluster of variable composition and orientation. Possible fillings are suggested in grey.

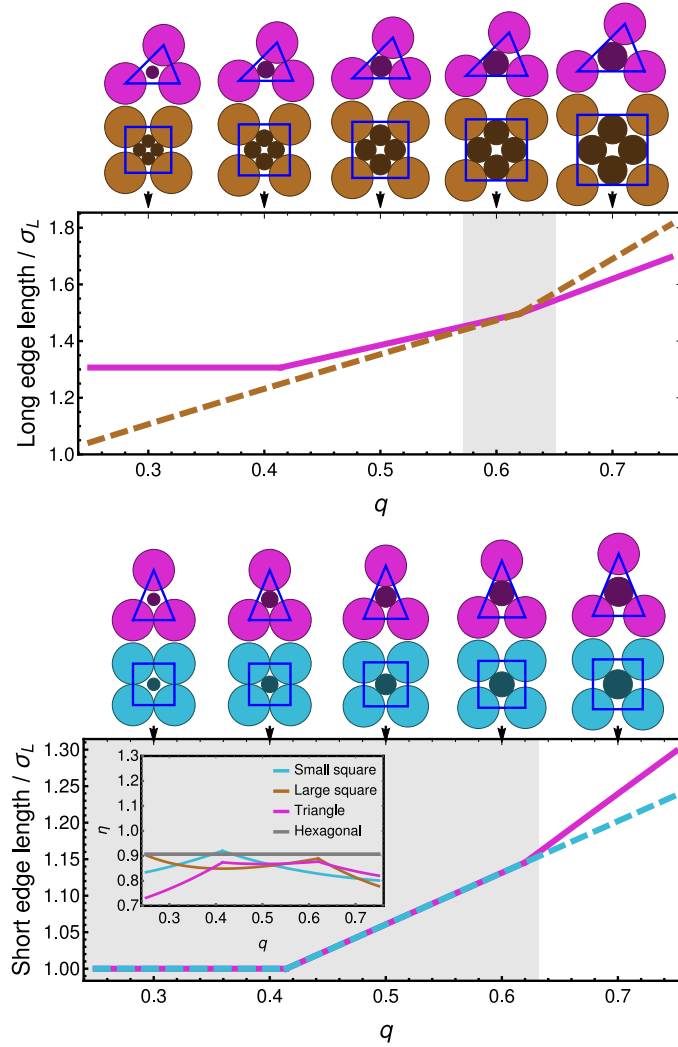


FIG. 6. Comparison of the long (top) and short (bottom) edge length of the tiles expected to form an octagonal quasicrystal in binary mixtures of *additive* hard disks. Size ratio intervals for which long or short edges match are highlighted with a darker background. The inset in the bottom graph displays the packing fraction of the various tiles as a function of size ratio, along with that of hexagonal packings.

ADDITIVE CASE

In complement to the main text analysis of spheres on a plane, which correspond to non-additive hard disks, we examine here the geometrical constraints in mixtures of *additive* hard disks, which cannot overlap (i.e., the non-additivity parameter is $\Delta = 0$). The 3D equivalent of this system would consist of spheres whose centers are constrained to lie in the same plane. Figure 6 shows the short and long edge lengths of the square and triangle tiles that can be formed with additive hard disks. While edge lengths could match for size ratios around $q = 0.6$, the inset graph shows that in this regime, the packing fraction of the tiles is systematically lower than that of hexagonal packing of large and small disks suggesting that the tiles are not dense enough to be stable in this system.

This observation was confirmed by simulating binary additive hard disk mixtures for size ratios between $q = 0.4$ and $q = 0.6$ in steps of 0.05, packing fractions between $\eta = 0.7$ and 0.9 in steps of 0.02, and compositions ranging from $x_S = 0.6$ to 0.9 in steps of 0.05. Quasicrystal self-assembly was observed in none of these simulations, although we cannot exclude the possibility of QC8 formation in longer simulation or different parameter regimes. As suggested by the above packing argument, many of the systems instead had a tendency to demix into separate large and small hexagonal domains. This is also consistent with the sparsity of stable binary crystal structures found at infinite

pressure for additive hard disks in this regime [10, 11].

-
- [1] M. Oxborrow and C. L. Henley, Random square-triangle tilings: A model for twelvefold-symmetric quasicrystals, *Phys. Rev. B* **48**, 6966 (1993).
 - [2] M. Impéror-Clerc, A. Jagannathan, P. Kalugin, and J.-F. Sadoc, Square-triangle tilings: an infinite playground for soft matter, *Soft Matter* **17**, 9560 (2021).
 - [3] M. Baake, D. Eciya, and U. Grimm, A guide to lifting aperiodic structures, *Z. Kristallogr. Cryst. Mater* **231**, 507 (2016).
 - [4] M. Zu, P. Tan, and N. Xu, Forming quasicrystals by monodisperse soft core particles, *Nature Communications* **8**, 1 (2017).
 - [5] B. Nienhuis, Exact solution of random tiling models, *Phys. Rep.* **301**, 271 (1998).
 - [6] R. Ammann, B. Grünbaum, and G. C. Shephard, Aperiodic tiles, *Discrete Comput. Geom.* **8**, 1 (1992).
 - [7] Y. Watanabe, M. Ito, and T. Soma, Nonperiodic tessellation with eightfold rotational symmetry, *Acta Crystallogr. A* **43**, 133 (1987).
 - [8] D. Joseph and V. Elser, A Model of Quasicrystal Growth, *Phys. Rev. Lett.* **79**, 1066 (1997).
 - [9] K. Je, S. Lee, E. G. Teich, M. Engel, and S. C. Glotzer, Entropic formation of a thermodynamically stable colloidal quasicrystal with negligible phason strain, *Proc. Natl. Acad. Sci. U.S.A.* **118**, e2011799118 (2021).
 - [10] C. Likos and C. Henley, Complex alloy phases for binary hard-disc mixtures, *Phil. Mag. B* **68**, 85 (1993).
 - [11] E. Fayen, A. Jagannathan, G. Foffi, and F. Smallenburg, Infinite-pressure phase diagram of binary mixtures of (non) additive hard disks, *J. Chem. Phys.* **152**, 204901 (2020).